Check for updates

Received: 27 May 2023 | Revised: 5 September 2023 | Accepted: 6 September 2023

DOI: 10.1002/eqe.4015

RESEARCH ARTICLE

WILEY

# Risk-based optimization of concentrically braced tall timber buildings: Derivative free optimization algorithm

**Raffaele Laguardia**[1] | **Paolo Franchin**[1] | **Solomon Tesfamariam**[2]

[1]Dipartimento di Ingegneria Strutturale e Geotecnica, Sapienza Universitá di Roma, Roma, Italy

[2]Department of Civil and Environmental Engineering, University of Waterloo, Waterloo, Canada

**Correspondence**
Raffaele Laguardia, Dipartimento di Ingegneria Strutturale e Geotecnica, Sapienza Universitá di Roma, Via Gramsci 53, 00197, Roma, Italy.
Email: raffaele.laguardia@uniroma1.it

**Funding information**
Natural Science Engineering Research Council of Canada, Grant/Award Number: RGPIN-2019-05013

**Abstract**

Mass timber materials are attractive alternatives for tall-timber buildings (TBs), where the need for sustainability is apparent. Innovative structural systems and design methodologies are needed to fulfil performance requirements according to modern performance based approaches. This paper deals with the design and optimization of buckling restrained braces as earthquake protection system for tall-TBs through risk-based design procedure. This procedure controls the mean annual frequency of exceedance of several limit states evaluated through a SAC-FEMA approach and using response spectrum linear analyses on linearized models for demand assessment. The features of the optimization procedure and the linearized models are shown through an application on a 20-story mass-TB located in a high seismic zone. The optimization is executed through a derivative-free algorithm, the generalized pattern Search, adopting several solution strategies whose efficiency and effectiveness for this kind of applications are shown and discussed. Finally, the results are compared and validated through the execution of non-linear analyses within a multiple stripe framework.

**KEYWORDS**

dissipative bracing, generalized pattern search, linearized models, risk-based design, tall timber buildings

## 1 | INTRODUCTION

With introduction of mass-timber, for example, glue-laminated timber (GLT), cross-laminated timber (CLT), timber is increasingly utilized construction material for the development of multi-story buildings.[1,2] As a result, tall timber buildings (TBs) have become viable and effective solution to meet sustainability objectives.[1,3] With the demand for innovation and resiliency, the research is now oriented towards the study of tall TBs in order to provide new proposal and solutions for their design and execution.[4–6] International codes are supporting this development, such as the Canadian National Building Code (NBC)[7] and 2021 International Building Code (IBC)[8] which now allow TBs up to 12 and 18 stories, respectively. One of the most challenging topics on tall TBs is their performance under strong wind and earthquake loads[6,9] and thus the development of new protection techniques and performance-based design methodologies suitable for the case of tall TBs. Tall TBs have intrinsically higher deformability, consequently, stiffness and resistance to lateral loads are commonly

This is an open access article under the terms of the Creative Commons Attribution-NonCommercial License, which permits use, distribution and reproduction in any medium, provided the original work is properly cited and is not used for commercial purposes.
© 2023 The Authors. *Earthquake Engineering & Structural Dynamics* published by John Wiley & Sons Ltd.

provided by shear walls or bracing systems. These elements are often realized in concrete or steel, thus obtaining hybrid structures, moreover they are often supplemented by energy dissipation mechanisms.[10,11] Possible application of bracing systems in tall TBs[12–15] is an attractive alternative as it can easily mitigate the weaknesses about stiffness and energy dissipation. For these reasons, this paper deals with risk-based optimal design of bracing systems for tall TBs.

Research on optimal bracing design has been ongoing for several years.[16–18] Despite the first optimization algorithms dating back to 1980's, the literature is continuously growing and updating. This is a result of the evolution of calculation methods and tools, available technologies and design philosophies lead to an unavoidable enhancement and development request also of well established methods. In the 1990's, Filiatrault & Cherry[19] and Ciampi et al.[20] proposed optimal design approaches to maximize dissipated energy or minimize structural damage based on numerical analyses on single-degree of freedom (SDOF) systems. Takewaki[21] proposed a procedure for multi-degree of freedom (MDOF) systems that allows minimization of interstory drift while constraining the maximum dissipated energy provided to the system through viscoelastic devices. Garcia[22] proposed a procedure for minimizing the added damping for structures with linear behavior using a Simplified Sequential Search Algorithm (SSSA). Levy et al.[23] proposed a two-step procedure to control the maximum displacement through time-domain linear analyses and derivative algorithms. Moreschi and Singh[24] proposed a procedure for optimal location of metallic and friction dampers using genetic algorithms and time-domain analysis. Lavan and Dargush[25] proposed a multi-objective optimization for bracing to control maximum drift and accelerations with a genetic algorithm and Pareto front. Pollini et al.[26] developed a procedure to minimize intervention cost of retrofitting interventions through viscoelastic device, time-domain analyses and gradient-based algorithms. Braga et al.[27] proposed a procedure to minimize intervention costs while constraining interstory drift and using Response Spectrum Analyses (RSAs) on linearized models and gradient-based algorithms. Laguardia and Franchin[28] developed a risk-based procedure that minimize the mean-annual frequency (MAF) of exceedance for several Limit States (LSs) on reinforced-concrete (RC) structure retrofitted with Buckling Restrained Braces (BRBs). A gradient based algorithms was used for RSAs on linearized models. Tu et al.[29] proposed an optimization procedure for BRBs optimal design based on modal and pushover analyses using a multi-objective genetic algorithm. Mazdarani et al.[30] proposed a reliability-based procedure for the optimal placement of bracing while minimizing the weight of the structure and using Enhanced Vibrating Particles System metaheuristic algorithm. As it can be noted, on the bracing design topic there are many contributions based on time-domain analyses and traditional Engineering Demand Parameters (EDPs) acceptance criteria (e.g., drift, accelerations, etc.). Only recently, some methods have been oriented to more practice-oriented approaches (e.g., using linear or non-linear static analyses) and, most of all, such recent methods are explicitly based on risk-based or reliability-based approaches, more in line with modern PBD concepts. As far as the optimization algorithm is concerned, derivative and genetic algorithm are mostly adopted. The derivative algorithm have some drawbacks in case of non-convex function or when gradients are hard to assess, while the genetic algorithm may be highly time-consuming. Nevertheless, the optimal design procedure available are mainly developed for RC and steel buildings and only recently some applications to TBs have been published but are limited to topological optimization[31] and SDOF approaches.[32]

This paper deals with the design of BRBs as earthquake protection system for tall TBs. To do so, a risk-based optimization procedure for bracing system design, originally developed for RC buildings,[28] is extended to TBs. The main feature of this procedure is providing brace properties satisfying performance requirements in terms of MAF exceedance of several LSs assessed through a SAC-FEMA approach[33] and seismic demand is assessed via elastic linear analyses on linearized models. In the Laguardia and Franchin,[28] the procedure has been applied to existing RC mid-rise buildings and using a gradient based algorithm. In this work the procedure is extended to tall TBs, using derivative free optimization algorithm, Generalized pattern search (GPS). In addition, a model of the brace that provide a significant reduction of the number of independent variables of the problem is utilized.

According to this, this paper set the following objectives:

- Present the design procedure for the applications to tall TBs.
- Discuss the effectiveness of derivative free algorithms for the solution of the problem through a parametric analyses that highlights the impact on the solution of trigger points and iteration criteria adopted.
- Validate the effectiveness of the solutions obtained within the method with Multiple Stripe Analyses (MSAs).[34]

The study is structured as follows. Section 2 presents the optimization problem and the adopted structural models for the case of a real tall TB case study. Section 3 provides a brief description of derivative free algorithms and GPS in particular. Section 4 presents the results of the procedure on the case study, in this section is also discussed the impact on the solution of the input parameters and convergence iteration criteria of GPS. Section 5 presents the comparison in terms

10969845, 0, Downloaded from https://onlinelibrary.wiley.com/doi/10.1002/eqe.4015 by CochraneItalia, Wiley Online Library on [23/09/2023]. See the Terms and Conditions (https://onlinelibrary.wiley.com/terms-and-conditions) on Wiley Online Library for rules of use; OA articles are governed by the applicable Creative Commons License

of performance between the procedure and non-linear analyses executed within a MSA framework. Finally, Section 6 exposes the concluding remarks.

## 2 | METHODOLOGY

This paper presents an application to TBs of a design method for bracing systems already developed for RC buildings.[28] This method stems from an initial proposal for design of new RC buildings,[35,36] the idea is to perform optimization using an objective function that is related to MAFs of exceedance of multiple LSs while using an equivalent linear model for the structure.

One of the peculiarities of the method lies in the use of RSAs for the assessment of seismic demand. To do so, the inelastic behavior of the structure is described by using some linear equivalent models. This issue is delivered assessing an element-wise secant stiffness based on local demand, while the energy dissipated is firstly assessed locally and then assembled globally to provide an equivalent damping ratio according to a substitute structure approach.[37] In order to assess the seismic demand, the linearization is done for several Hazard Levels (HLs), thus providing several equivalent linear models and damping ratios. The other relevant feature of the method lies in the MAF assessment that is done, for each LS, according to the SAC-FEMA approach[33] with a second-order approximation of hazard.[38] A summary flowchart of the methodology is shown in Figure 1 and briefly described in the following

| **Risk-based optimal design procedure** |
|---|
| 1: Definition of the building properties. Input of geometry, materials, loads and connectivity. |
| 2: Seismic Hazard definition for the chosen site: input of a collection of Hazard Curves (HCs) for spectral accelerations for several periods or, alternatively, a collection of Uniform Hazard Spectra (UHS). |
| 3: Definition of parameters to be adopted as design variables and definition of an initial guess, $\mathbf{d}^{[1]}$. |
| 4: Setup of a FE model considering the independent variables properties at i-th design iteration (i.e., i-th point in the design space) for each of the $n_{HL}$ considered HLs. Assessment of the elastic fundamental period of the system $T_{el}^{[i]}$. |
| 5: RSAs on the FE models set in step 4 and output of the local displacement demand on the m-th brace for the l-th hazard level, $u_{B,m}^{[i,l]}$, to be used as input for the linearization process. |
| 6: Linearization process: member-wise dissipated energy, $E_{d,m}^{[i,l]}$ and secant stiffness,$K_{eq,m}^{[i,l]}$ assessment. Calculation of global equivalent damping ratio, $\xi_{eq}^{[i,l]}$. |
| 7: Update of FE models by using secant stiffness and damping ratios coming from step 6. |
| 8: RSAs on the updated FE models and output of chord rotation demands, $\theta_{max}^{[i,l]}$, for all the HLs. |
| 9: Median demand interpolation and assessment of seismic demand parameters $a^{[i]}$ and $b^{[i]}$. |
| 10: Definition of HC for the $T_{el}^{[i]}$ and output of $\lambda\left[S_a(T_{el}^{[i]})\right]$. |
| 11: HC interpolation and output of hazard parameters $k_0^{[i]}, k_1^{[i]}, k_2^{[i]}$. |
| 12: Closed form MAF according to Equation (7b). |
| 13: Check of convergence on a minimum value of the Objective Function |

In the present work it will be shown the application of this procedure for the optimal design of BRBs on tall TBs through an application on a real case study. Specifically, Section 2.1 describes the TB adopted as a case study and the input parameters required for the procedure (Step 1). Section 2.2 describes the Hazard input adopted for this application (Step 2). Section 2.3 describes the modeling assumptions, the independent variables and the linearization schemes adopted (Steps 3–8). Section 2.4 introduces briefly the MAF assessment performed through a SAC-FEMA approach with second-order hazard approximation (Steps 9–12). Finally, in Section 2.5 the optimization problem for this application is formalized (Step 13).

### 2.1 | Building properties input

The procedure depicted above is applied to a real tall TBs, the 20 storey high Museum Tower Apartment Building located in Los Angeles (California, USA). This building has been designed and realized with an RC structure but recently a review of the project has been proposed, thinking at at the same building but with a mass timber structure.[39] In this paper,

10969845, 0, Downloaded from https://onlinelibrary.wiley.com/doi/10.1002/eqe.4015 by CochraneItalia, Wiley Online Library on [23/09/2023]. See the Terms and Conditions (https://onlinelibrary.wiley.com/terms-and-conditions) on Wiley Online Library for rules of use; OA articles are governed by the applicable Creative Commons License

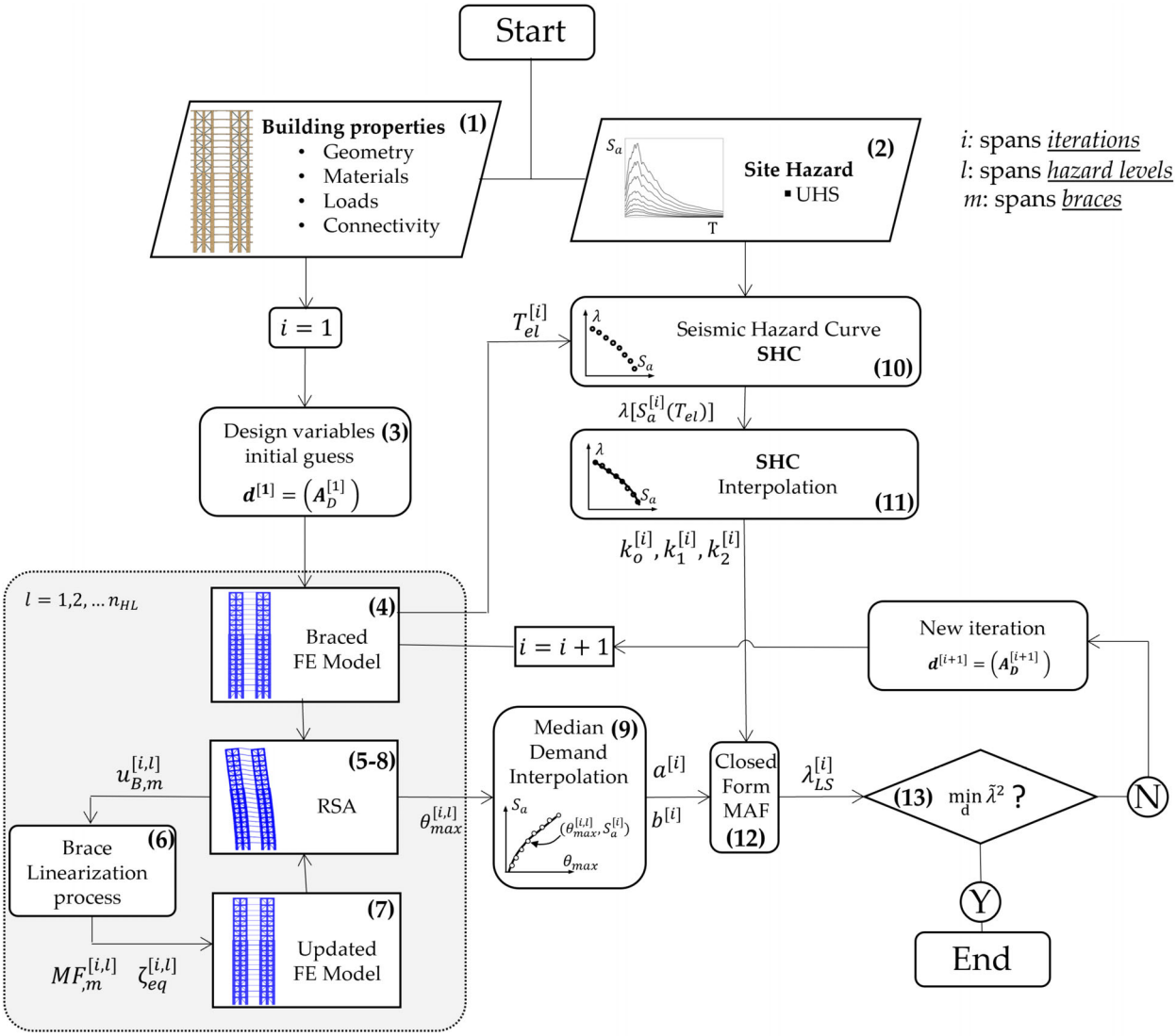


**FIGURE 1** Flowchart of the procedure.

the application is limited to a 2D portion of the building, shown in Figure 2B and corresponding to the alignment 1 of the whole building, as can be seen in the plan view of Figure 2B. Each braced frame has GluLam beams with section 365 mm × 684 mm pinned to vertical GluLam columns with section equal to 1520 mm × 365 mm for the first 10 floors and a section 912 mm × 365 mm for the last 10 floors. Columns and beams are made of Glulam grade DFL [1]-16c-E and DFL[1]-20c-E, respectively. As far as masses are concerned, in Figure 2B it can be noticed that the original building has 12 braced frames, six for each principal direction, of whom four on peripheral frames and two on internal frames. Accordingly and assuming an homogeneous partition among braced frames of seismic loads, a mass of 1/3 of the total mass of the building is applied at each floor of the 2D model. The total weight of the building according to this approach is 31016 kN.

## 2.2 | Structural model

This section describes the structural model adopted within the procedure. The interest is about the use of BRBs on a tall TB. This type of brace has been widely studied and adopted[40–44] and it's characterized by a non-buckling behavior

[1] DFL stands for Douglas Fir-larch

10969845, 0, Downloaded from https://onlinelibrary.wiley.com/doi/10.1002/eqe.4015 by CochraneItalia, Wiley Online Library on [23/09/2023]. See the Terms and Conditions (https://onlinelibrary.wiley.com/terms-and-conditions) on Wiley Online Library for rules of use; OA articles are governed by the applicable Creative Commons License

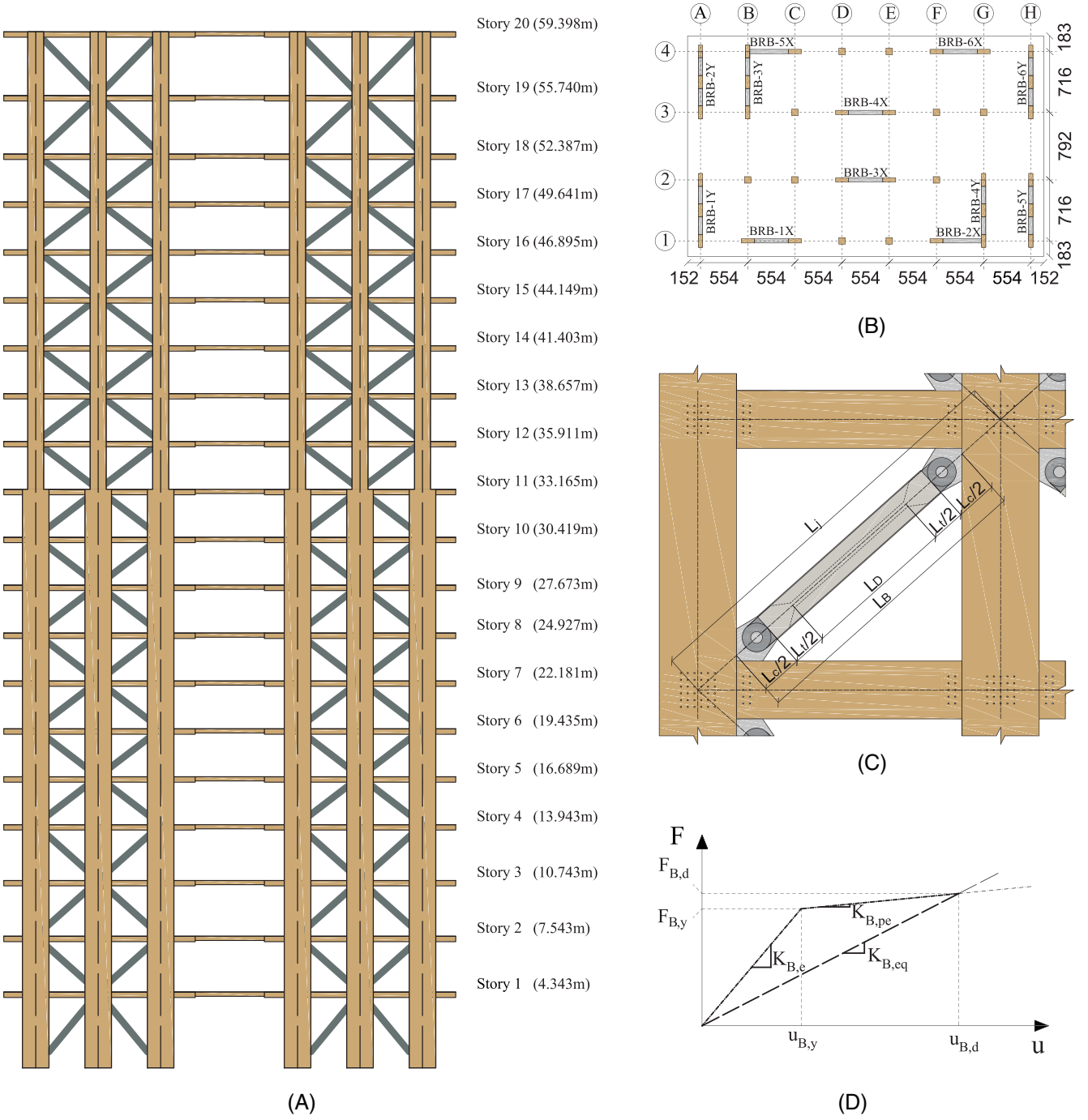


**FIGURE 2** (A)Braces elevation arrangement on the case study; (B) plan view of the case study; (C) detail of BRB components arrangement; (D) Backbone curve adopted for BRB modeling. BRB, Buckling Restrained Brace.

typically achieved by encasing a steel core in a concrete-filled tube that avoids buckling mechanisms. The Non-Linear BRBs behavior is elastoplastic hardening with a slight asymmetrical behavior between tension and compression,[45] within the literature there are many specialized models for the description of such a behavior.[45,46] In this work, given the use of linear analysis, the BRB is modeled exclusively through its elastic-hardening backbone curve, thus assuming the same behavior in tension and compression. The arrangement of a typical BRB is shown in Figure 2C, it is composed by a zone intended for dissipation with length $L_D$, a transition zone with length $L_t$, and a connection zone with length $L_c$. In Figure 2C the full length of the brace, $L_B$, and the joint-to joint distance,$L_j$, are also indicated. The different parts of the brace have different areas, for this reason the elastic stiffness of the brace, $K_{B,e}$, is defined considering a series arrangement of the three parts[47]:

10969845, 0, Downloaded from https://onlinelibrary.wiley.com/doi/10.1002/eqe.4015 by CochraneItalia, Wiley Online Library on [23/09/2023]. See the Terms and Conditions (https://onlinelibrary.wiley.com/terms-and-conditions) on Wiley Online Library for rules of use; OA articles are governed by the applicable Creative Commons License

$$A_{B,e} = \frac{L_B}{\frac{L_D}{A_D} + \frac{L_t}{A_t} + \frac{L_c}{A_c}} = \frac{L_B A_D}{L_D + L_t \frac{A_D}{A_t} + L_c \frac{A_D}{A_c}} \tag{1a}$$

$$K_{B,e} = \frac{E_s A_{B,e}}{L_B} \tag{1b}$$

where $A_{B,e}$ is the equivalent brace area, $A_c, A_t$ and $A_D$ are the areas of connection, transition and dissipative zones, respectively, and $E_s$ is the steel Young's modulus.

The post-elastic stiffness of the brace can be defined using the same approach and assuming that the yielding is limited to dissipative zone, thus assuming a reduced stiffness only for that zone

$$A_{B,pe} = \frac{L_B}{\frac{L_D}{rA_D} + \frac{L_t}{A_t} + \frac{L_c}{A_c}} = \frac{L_B r A_D}{L_D + L_t \frac{rA_D}{A_t} + L_c \frac{rA_D}{A_c}} \tag{1c}$$

$$K_{B,pe} = \frac{E_s A_{B,pe}}{L_B} \tag{1d}$$

where $A_{B,pe}$ is the equivalent brace area in the post-elastic field and $r$ is the steel hardening ratio.

The full backbone curve of the brace is depicted in Figure 2D and can be defined according to the following expressions

$$F_{B,y} = A_D f_y \tag{2a}$$

$$u_{B,y} = \frac{F_{B,y}}{K_{B,e}} \tag{2b}$$

$$F_{B,d} = F_{B,y} + (u_{B,d} - u_{B,y}) K_{B,pe} \quad \text{if } u_{B,d} > u_{B,y} \tag{2c}$$

$$F_{B,d} = u_d K_{B,e} \quad \text{if } u_{B,d} \leq u_{B,y} \tag{2d}$$

$$K_{B,eq} = \frac{F_{B,d}}{u_{B,d}} \tag{2e}$$

$$E_{B,d} = 4(F_{B,y} u_d - F_{B,d} u_{B,y}) \quad \text{if } u_{B,d} > u_{B,y} \tag{2f}$$

$$E_{B,d} = 0 \quad \text{if } u_d \leq u_{B,y} \tag{2g}$$

where $f_y$ is the steel yielding stress, $F_{B,y}$ is the brace yielding force, $u_d$ is the displacement demand, $F_{B,d}$ is the brace force at the displacement demand, $K_{B,eq}$ is the equivalent secant stiffness at the displacement demand and $E_{B,d}$ is the dissipated energy at the displacement demand.

By observing Equations (1), (2) it is clear that the yielding force of BRB depends upon its dissipative zone area while the stiffness depends upon the areas and lengths of all the three zones (i.e., dissipative, transition and connection). In particular, the length of the dissipative zone highly influence the stiffness of the system and indeed some BRBs with a reduced length of the dissipative zone have been object of investigations of some research works[47–50] and have also been adopted in several real case applications.[51,52] However, the parameter that mainly influences the response is the area of the dissipative zone, $A_D$, while the adoption of the other parameters as independent variables of the optimization doesn't provide significant advantages in terms of device optimization.[28] Based on this considerations only the area of dissipative zone (i.e., $A_D$) will be considered as independent variable while the remaining characteristics of each brace are fixed and defined according to typical BRBs arrangement schemes. For this application, the following values are adopted[47]:

$$L_t = 500mm \qquad L_c = 1300mm \tag{3a}$$

$$\frac{A_D}{A_t} = 0.5 \qquad \frac{A_D}{A_c} = 0.3 \tag{3b}$$

10969845, 0, Downloaded from https://onlinelibrary.wiley.com/doi/10.1002/eqe.4015 by CochraneItalia, Wiley Online Library on [23/09/2023]. See the Terms and Conditions (https://onlinelibrary.wiley.com/terms-and-conditions) on Wiley Online Library for rules of use; OA articles are governed by the applicable Creative Commons License

As far as the timber structure is concerned, when it is designed as a moment-resisting frame, plasticity and energy dissipation are provided by connections, while timber members are designed to remain elastic. In this case, connections stiffness.[53,54] plays a crucial role in structural response assessment. In the case study, however, the adopted lateral resisting system is a concentric braced frame, where lateral forces are almost exclusively born by the braces. Figure 2C shows the beam to column connection adopted in this work: its stiffness is lower than 2 MNm that is negligible when compared to the bending stiffness of the adjoining timber members and also much lower than typical values for the case of deformable beam to column connection.[53] For these reasons, the beam to column connections are modeled as pinned, braces are considered to resist the entire lateral load and timber members are elastic by design. Accordingly, no energy dissipation is provided by the timber component of the structural system.

Crucial to the feasibility of the BRB configuration, however, is that connections of adequate strength and stiffness to transmit the resulting brace forces can be designed without damage to the timber. Doweled connections are considered in this paper, as shown in Figure 2C. A good overview of the design issues for doweled and screwed connections in BRB-timber applications is given by Dong et al.[55] Critical issues, as already mentioned, concern the connection strength and stiffness. Considering the conventional assumptions made for assembling the BRB stiffness from its parts, the connection stiffness can be neglected. On the other hand, a connection strength-deficit would translate in a design constraint to be considered in the procedure. For the sake of simplicity, this design constraint is checked at the end to verify the feasibility of the optimization solution. Technically, and without loss of generality, a maximum BRB force is determined, compatible with the adjoining timber members, according to the code prescriptions of Eurocode 5.[56]

By considering the brace arrangement of Figure 2A, the connections with highest demand are on the external column of the braced frame where a big vertical load is transferred to the column. Figure 2C shows a possible dowel connection arrangement with 36 dowels. Assuming a dowel diameter $d = 16$ mm with an ultimate characteristics strength $f_{u,k} = 355$ MPa, two inner gusset plate embedded in the timber with thickness $t_p = 20$ mm, timber element thickness $t_1 = t_2 = 91$ mm with characteristics yielding stress $f_{y,k} = 275$ MPa, the ultimate strength capacity of the connection is equal to 1499 kN.

As already mentioned, the seismic demand assessment is obtained performing RSAs for several LSs on a FE model. In that models the brace linearization is considered modifying the stiffness of each brace element through some Modification Factors (MFs) and reducing the spectral ordinates using a global equivalent damping ratio evaluated according to a substitute structure approach.[37]

The MFs are formalized as follows:

$$MF = \frac{K_{eq}}{K_0} \tag{4a}$$

$$K_0 = \frac{E_s A_{ref}}{L_B} \tag{4b}$$

where $K_0$ is a reference stiffness obtained assuming a brace with a reference area $A_{ref}$.

As far as the equivalent damping ratio is concerned, it is obtained according to the approach proposed by Jacobsen[57,58] through the following expression

$$\xi_{eq} = \xi_h + \xi_v = \frac{1}{4\pi} \frac{\sum_m E_{Bd,m}}{E_{el}} + \xi_v \tag{5}$$

where $m$ spans the number of braces, $\xi_h$ is the equivalent damping due to hysteresis, $\xi_v$ is the inherent viscous damping, $E_{el}$ is the elastic energy of the system computed as $E_{el} = T_{max} u_{max}/2$, where $T_{max}$ is the maximum base shear and $u_{max}$ is the maximum top displacement of the system. Please note that $\xi_{eq}$ is expressed in percentage. By using Equation (5) the final damping contribution is obtained as the sum of a hysteretic term and an inherent elastic one, the first obtained on the basis of the work done by each brace, while the second calibrated considering structural typology and properties of the building.[59–61]

The damping ratio is considered within the RSA by reducing the spectral ordinates according to the following expression[62]

$$\eta = \sqrt{\frac{10}{5 + \xi_{eq}}} \tag{6}$$

10969845, 0, Downloaded from https://onlinelibrary.wiley.com/doi/10.1002/eqe.4015 by CochraneItalia, Wiley Online Library on [23/09/2023]. See the Terms and Conditions (https://onlinelibrary.wiley.com/terms-and-conditions) on Wiley Online Library for rules of use; OA articles are governed by the applicable Creative Commons License

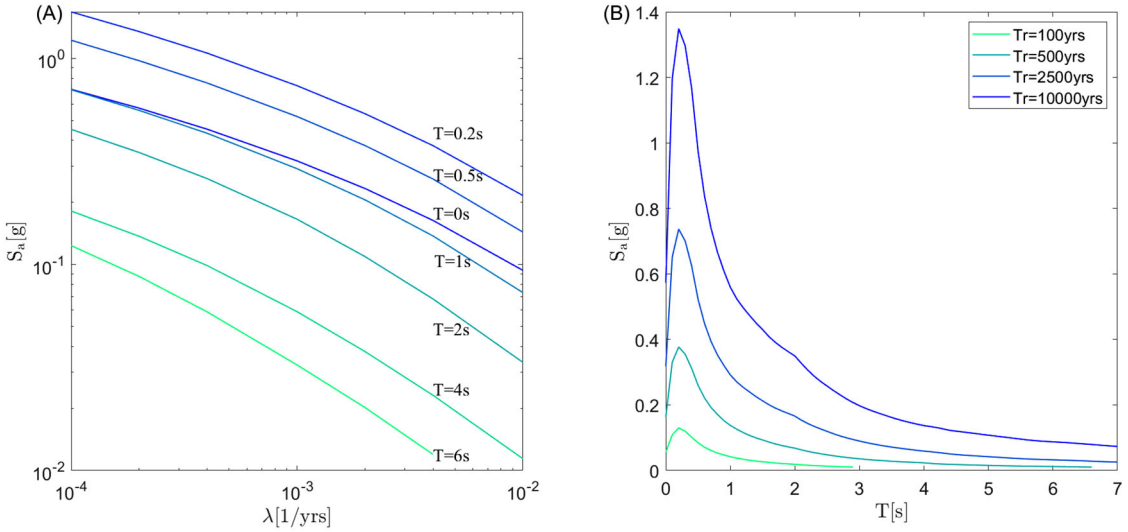


**FIGURE 3** Hazard data for the site of Vancouver (LAT 49.25 LON -123.12): (A) HCs for several periods, (B) UHS for four return periods. HCs, Hazard Curves; UHS, Uniform Hazard Spectra.

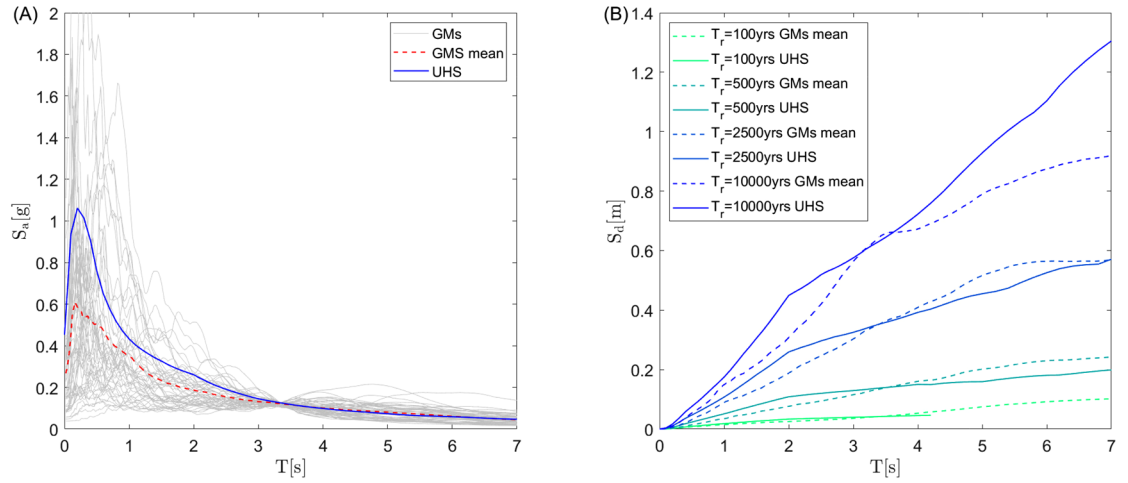


**FIGURE 4** GMs selection for the site of Vancouver (LAT 49.25 LON -123.12): (A) Comparison of GMs spectra, their mean and UHS for an HL with $T_r$=2500 yrs, (B) Displacement spectra for four return periods, comparison of UHS and GMs mean. GMs, Ground Motions; HCs, Hazard Curves; UHS, Uniform Hazard Spectra.

## 2.3 | Hazard input

The step 2 of the procedure requires the input of the HC assessed in correspondance of the building site. In this application the hazard of the city of Vancouver (i.e., LAT 49.25 LON -123.12) and a soil type C according to Canadian Building Code[7] are adopted. The hazard information are extrapolated using the OpenQuake engine[63] and the data of 6th generation Seismic Hazard Model (SHM6) for Canada.[64] In Figure 3 are shown the Seismic HCs adopted and the response spectra for four return periods (i.e., $T_r$=100, 500, 2500 and 10,000 yrs). The Ground Motions (GMs) selection has been carried out in order to be consistent with the actual major seismic sources (crustal, inslab, and interface) that most significantly contribute to the hazard of the Vancouver region. Accordingly, a Conditional Mean Spectrum (CMS) based record selection method[65] is used to select several suite of GM records that possess key features (e.g. magnitude, frequency content, and duration) of the considered seismic sources.[66] Within this approach, one CMS is assessed for each involved seismic source and the number of GMs matched on each CMS is proportional to the hazard percentage contribution of that source. Hence, a set of 50 GM records (bi-directional) have been selected at the anchor period of $T_e = 3.35s$, and to be consistent with seven HLs (i.e. $T_r$ =100, 250, 500, 1000, 2500, 5000, 10,000 yrs). Figure 4A shows the GMs set selected for $T_r$ = 24754 yrs and

10969845, 0, Downloaded from https://onlinelibrary.wiley.com/doi/10.1002/eqe.4015 by CochraneItalia, Wiley Online Library on [23/09/2023]. See the Terms and Conditions (https://onlinelibrary.wiley.com/terms-and-conditions) on Wiley Online Library for rules of use; OA articles are governed by the applicable Creative Commons License

**TABLE 1** Median values of peak IDR, total demand dispersion and total capacity dispersion for LD and CP LSs.

| LD | | | CP | | |
|---|---|---|---|---|---|
| $\theta_{max}$ | $\beta_{D,T}$ | $\beta_{C,T}$ | $\theta_{max}$ | $\beta_{D,T}$ | $\beta_{C,T}$ |
| 0.005 | 0.3 | 0.0 | 0.025 | 0.3 | 0.5 |

Abbreviations: CP, Collapse Prevention; IDR, Interstory Drift Ratio; LD, Light Damage; LSs, Limit States.

the related UHS. Finally, Figure 4B also shows the comparison of the displacement spectra coming from PSHA and the mean spectra of the GMs set for four HLs in order to highlight the different displacement demand corresponding to the two hazard descriptions, which are used in the RSA and the MSA, respectively, and help explaining differences found in validation and shown later (see Section 4).

## 2.4 | MAF assessment

Within the optimization procedure the performance is described through the MAF assessment for several LSs. MAF is assessed by using a SAC-FEMA approach[33] with a second-order approximation of Hazard[38] according to the following expressions

$$\lambda_{IM} = k_0 \exp\left(-k_2 ln(x)^2 - k_1 ln(x)\right) \tag{7a}$$

$$\lambda_{LS} = \sqrt{\phi} k_0^{1-\phi} \left\{ \lambda_{IM} \left[ \left( \frac{\hat{C}}{a} \right)^{1/b} \right] \right\}^{\phi} \exp\left[ \frac{k_1^2}{4k_2} (1 - \Phi) \right] \tag{7b}$$

$$\phi = \frac{1}{1 + 2k_2 \left( \beta_{D,T}^2 + \beta_{C,T}^2 \right) / b^2} \tag{7c}$$

where $\lambda_{IM}$ is the MAF of Intensity Measure (IM) derived from Hazard, $k_0$, $k_1$ and $k_2$ are the second-order hazard interpolation parameters and $x$ is the IM value. $\lambda_{LS}$ is the MAF for a LS, $\hat{C}$ is the median LS capacity, $a$ and $b$ are the parameters governing the seismic demand expressed according to the following power law $\hat{D} = ax^b$, whereas $\beta_{D,T}$ and $\beta_{C,T}$ are the total demand and capacity dispersions.

As far as this application is concerned, the adopted demand parameter is the Interstory Drift Ratio (IDR), denoted with the symbol $\theta$ associated with member chord rotation. Two LSs have been considered, Light Damage (LD) and Collapse Prevention (CP). The definition of median values and dispersions is crucial for the final assessment of the procedure, while not investigating the effect of such parameters on the final assessment, some credible values consistent with Canadian Building Code requirements[67] for median values and other consolidated literature for the dispersion values[68,69] are adopted and summarized in Table 1.

# 3 | OPTIMIZATION ALGORITHMS

The engineering problem described in Section 3.1 is a Non-Linear (NL) unconstrained one, given the NL relationship between variables and Objective Function (OF) and the contemporary absence of constraints. To solve that problem the choice of the optimization algorithm, among the many available, is crucial to obtain an effective solution and an efficient procedure. In case optimization problem is convex, the straightforward solution is using gradient-based algorithms where the solution is iteratively found by moving on the OF surface and finding the best search direction through gradients assessment. These algorithms require that the OF is differentiable and are very effective if the gradients are well-known or numerically easy to assess. When this is not true, other algorithms should be preferred. In the optimization problem described in Equation (9), the objective function is non-linear and non-convex, furthermore its gradients as a function of the variables are not known a-priori but must be derived numerically with an important computational effort and many structural analyses required, thus gradient-based algorithms appear as poorly suitable for that problem. In the recent years many algorithms that avoid the gradients assessment are used under the name of "derivative free" algorithms. A comprehensive survey of such methods is given in ref. [70] where the derivative free algorithms are classified in the following sets: evolutionary algorithms, physical algorithms, swarm algorithms and Direct Search Algorithms (DSAs).

10969845, 0, Downloaded from https://onlinelibrary.wiley.com/doi/10.1002/eqe.4015 by CochraneItalia, Wiley Online Library on [23/09/2023]. See the Terms and Conditions (https://onlinelibrary.wiley.com/terms-and-conditions) on Wiley Online Library for rules of use; OA articles are governed by the applicable Creative Commons License

Among the DSAs, Directional Direct Search algorithms (DDSAs) have been adopted in this work and their characteristics are briefly presented in the next paragraphs.

## 3.1 | Objective function

The optimization problem herein adopted aims at the definition of a bracing system that fulfil specific performance requirements expressed in terms of risk parameters. To do so, a function $\tilde{\lambda}$ has been defined,[28] it allows the control of the risk level being a function of the MAF of exceedance for $n_{LS}$ LSs. It can be defined as the 'distance' from the threshold for the governing LS, that is, the LS that, in each optimization step, is the closest to its corresponding threshold $\lambda^*_{LS}$:

$$\tilde{\lambda}(\mathbf{d}) = max_k\left(\frac{\lambda_{LS,k}(\mathbf{d})}{\lambda^*_{LS}} - 1\right) \qquad k = 1, 2, \dots, n_{LS} \tag{8}$$

The objective function is the squared valued of Equation 8, $\tilde{\lambda}^2$ and no constraints on independent variable are provided. The advantage of using the squared value of $\tilde{\lambda}$ lies in the fact that it is always positive and exactly equal to zero when the MAF of one LS is equal to the threshold value and the MAFs of other LSs are lower than their thresholds. The optimization problem can then be formulated as follows

$$\text{find} \qquad \min_{\mathbf{d}} \tilde{\lambda}^2 \tag{9}$$

## 3.2 | Derivative free - DDS algorithms

DDSAs are based on a very simple idea: starting from an initial point,$\mathbf{d}^{[1]}$ , the surroundings of that point are investigated to search a new point , $\mathbf{d}^{[2]}$, where the objective function value is lower than on initial point; a minimum of the OF is reached iterating this way. The several DDSAs differ from each other for the way the search is performed, two key features are the direction and amplitude of the search. The first algorithm of this kind was the Coordinate Search Algorithm (CSA),[71] it looks for the solution around the incumbent point with fixed directions and amplitudes. A relevant evolution of CSA is the Generalized Pattern search (GPS)[72] which introduce two enhancements: search direction can change from iteration to iteration and search is not limited only around the incumbent solution. Accordingly, the procedure is divided into "Poll" steps, when search is done around incumbent, and into "Search" steps when search is done with other criteria. A key concept of GPS is the "Mesh", it is a grid of points from which the GPS algorithm selects candidate trial points and its size can change iteration after iteration. The pseudo-code of GPS algorithm can be expressed as in Algorithm 1.[73]

Using GPS, the choice of the correct solution strategy and initial point are primary aspects. As for the strategies, it is possible to adopt some "Opportunistic Strategies" (OS), using them if during the polling or search phases the algorithm finds a point better than the incumbent solution (i.e., with a lower OF), it can stop and proceed to the next iteration without terminating the query of the other points. Accordingly, while using OS, the order of the points to be investigated on the mesh or, in other words, the order of the search directions, is crucial for the rapidity and effectiveness of the results. Within the MATLAB environment, the following OS are provided:

- *Consecutive*: Polling is done by querying the points using a fixed order of search directions.
- *Random*: Polling is done by querying the points using a randomly generated order of search direction.
- *Success*: Polling is done by querying the points starting from the direction that had success at the previous iteration, after the first query the polling continues according to a consecutive strategy.

Regarding the initial point, its choice can highly influence the reaching of the minimum and the speed of the process, it can be done according to the experience of the operator, or executing some pre-iteration step with some algorithms specifically developed for the initial point sampling (e.g. random, stratified, Latin Hypercube[74]).

GPS algorithm effectiveness is tested by investigating several initial trigger conditions and different solution strategies (i.e. "opportunistic" or not), as resumed in Table 2. The trigger case 'Constant' has the same initial area values at all the floors, while the 'Trapezoidal' case has initial area values that linearly reduce from the bottom to the top of the building with a ratio 3:1.

10969845, 0, Downloaded from https://onlinelibrary.wiley.com/doi/10.1002/eqe.4015 by CochraneItalia, Wiley Online Library on [23/09/2023]. See the Terms and Conditions (https://onlinelibrary.wiley.com/terms-and-conditions) on Wiley Online Library for rules of use; OA articles are governed by the applicable Creative Commons License

**ALGORITHM 1** Generalized Pattern Search (GPS).

Given $f : \mathbb{R}^n \to \mathbb{R}$ and starting point $d^{[1]} \in \mathbb{R}^n$

0. INITIALISATION

| | |
|---|---|
| $\delta^{[1]} \in (0, \text{inf})$ | initial mesh size parameter |
| $D = GZ$ | positive spanning matrix |
| $\tau \in (0, 1)$, with $\tau$ rational | mesh size adjustment parameter |
| $\epsilon_{stop} \in [0, \text{inf})$ | stopping tolerance |
| $k \leftarrow 0$ | iteration counter |

1.SEARCH

**if** $f(t) < f(d^{[k]})$ for some t in a finite subset $S^{[k]}$ of the mesh $M^{[k]}$ **then**

set $d^{[k+1]} \leftarrow t$ and $\delta^{[k+1]} \leftarrow \tau^{-1}\delta^{[k]}$ and go to 3

**else**

go to 2

**end if**

2.POLL

Select a positive spanning set $\mathbb{D}^{[k]} \subseteq \mathbb{D}$

**if** $f(t) < f(d^{[k]})$ for some t $\in P^{[k]} = \{d^{[k]} + \delta^{[k]}d : d \in \mathbb{D}^{[k]}\}$ **then**

set $d^{[k+1]} \leftarrow t$ and $\delta^{[k+1]} \leftarrow \tau^{-1}\delta^{[k]}$

**else** $d^{[k]}$ is a mesh local optimizer

set $d^{[k+1]} \leftarrow t$ and $\delta^{[k]} \leftarrow \tau\delta^{[k]}$

**end if**

3.TERMINATION

**if** $\delta^{[k+1]} > \epsilon_{stop}$ **then**

increment $k \leftarrow k + 1$ and go to 1

**else**

stop

**end if**

**TABLE 2** List of the considered cases adopted to solve the optimization problem using different strategies and initial points, $\mathbf{d^{[1]}}$.

| n. | Case | Algorithm | Strategy | $\mathbf{d^{[1]}}$ |
|---|---|---|---|---|
| 1 | $G_{1C}$ | GPS | Full-Poll | Constant |
| 2 | $G_{2C}$ | GPS | Random | Constant |
| 3 | $G_{3C}$ | GPS | Success | Constant |
| 4 | $G_{1T}$ | GPS | Full-Poll | Trapezoidal |
| 5 | $G_{2T}$ | GPS | Random | Trapezoidal |
| 6 | $G_{3T}$ | GPS | Success | Trapezoidal |

## 4 | RESULTS AND DISCUSSIONS

This section describes the solutions obtained with the methodology exposed in Section 2 by applying the optimization algorithm introduced in section 3 according to the different approaches illustrated in Table 2. The case study structure is equipped with 80 braces distributed among four braced frames. However, the number of independent variables is 20, one for each floor of the building, thus reasonably assuming that the braces of each frame have equal characteristics at the same floor.

Figure 5 shows the progress with the Function Counts (FCs) of OF ($\tilde{\lambda}^2$) and MAF of the two considered LS ($\lambda_{LD}$ and $\lambda_{CP}$). The FC number represents the times the OF is invoked or, in other words, the times the MAF is assessed for all the LSs. Furthermore, the total number of FCs are summarized in Table 3. Figures 5A,D show the $G_{1c}$ and $G_{1t}$ (i.e., "Full-Poll" cases) where convergence is obtained after 3161 and 2868 FCs, respectively. Figures 5B,E show the $G_{2c}$ and $G_{2t}$ (i.e.,

10969845, 0, Downloaded from https://onlinelibrary.wiley.com/doi/10.1002/eqe.4015 by CochraneItalia, Wiley Online Library on [23/09/2023]. See the Terms and Conditions (https://onlinelibrary.wiley.com/terms-and-conditions) on Wiley Online Library for rules of use; OA articles are governed by the applicable Creative Commons License

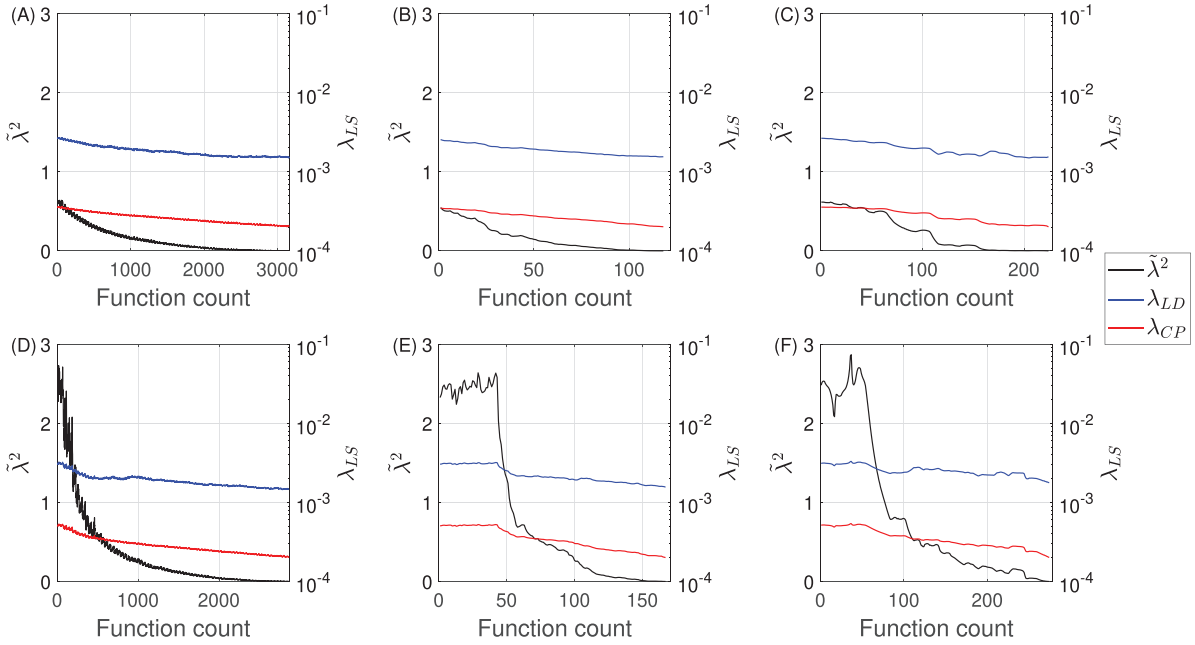


**FIGURE 5** $\tilde{\lambda}^2$, $\lambda_{LD}$ and $\lambda_{CP}$ values versus number of FCs: (A) Case $G_{1c}$; (B) Case $G_{2c}$; (C) Case $G_{3c}$; (D) Case $G_{1t}$; (E) Case $G_{2t}$; (F) Case $G_{3t}$. FCs, Function Counts.

**TABLE 3** Resume of design and performance values obtained for different optimization cases.

| | $G_{1C}$ | $G_{2C}$ | $G_{3C}$ | $G_{1T}$ | $G_{2T}$ | $G_{3T}$ |
|---|---|---|---|---|---|---|
| $F_{count}$ | 3161 | 122 | 228 | 2868 | 171 | 278 |
| $V[cm^3]$ | 50269 | 56406 | 61367 | 51731 | 61125 | 65561 |
| $\theta_{max,HL1}$ | 0.16% | 0.15% | 0.17% | 0.16% | 0.17% | 0.18% |
| $\theta_{max,HL2}$ | 0.43% | 0.44% | 0.49% | 0.44% | 0.52% | 0.452% |
| $\theta_{max,HL3}$ | 1.13% | 1.15% | 1.07% | 1.09% | 1.03% | 1.14% |
| $\theta_{max,HL4}$ | 3.06% | 3.04% | 3.02% | 3.14% | 3.05% | 2.89% |

"Random" OS cases), in these cases the FCs needed for convergence drastically reduce to 122 and 171, respectively. Figures 5C,F show the $G_{3c}$ and $G_{3t}$ cases (i.e., "Success" OS cases) when 228 FCs and 278 FCs are needed for convergence, respectively. By comparing the numerical values described above, it can be concluded that using OSs allows a reduction of required FCs of about an order of magnitude, with a slightly higher effectiveness of "Random" strategy. As an average, about 60 s for each FC are required on the computer adopted for this study, meaning that using a 'Full-Poll' strategy required 50 and 35 hours for the solution of $G_{1c}$ and $G_{1t}$ cases, respectively, while using OSs the resolution times have been comprised between 2 h ($G_{2c}$) and 4 h ($G_{3t}$), respectively. For the sake of comparison, in a previous work[28] where a gradient-based algorithm was adopted on a case study with five braces and 15 independent variables, the solution was obtained with 560 FCs. These numbers roughly show that derivative free algorithms tend to be slower than gradient-based algorithms in the case of a "Full-Poll" strategy but can become much faster and therefore profitable using OSs. Nevertheless, the initial point (i.e., Constant or Trapezoidal) doesn't significantly influence the convergence speed. Moreover, it should be observed that in all the cases the algorithm has stopped when the value of $\lambda_{CP}$ reached its acceptance criteria (i.e. $2 \times 10^{-4}$) while the $\lambda_{LD}$ value is much less than its acceptance value (i.e. $1 \times 10^{-2}$). On this point it should be considered that braced frames are stiffer than moment-resisting frames and their design is usually strength controlled rather than deformation controlled. As a results, CP rather than LD is the ruling requirement, consistently with the results obtained herein.

Figure 6 shows the final values of independent variables, $\mathbf{d}^{[\mathbf{f}]}$, compared with initial points, $\mathbf{d}^{[\mathbf{1}]}$, for all the investigated cases.

Figures 6A,D show the solutions for $G_{1c}$ and $G_{1t}$, in these cases the procedure provides a strong increase of the braces placed in the middle stories (i.e., 5–15) and also a slight increase of braces placed at the highest floors (i.e. 16–20), at the same time it can be noticed that the braces at the lowest floors (i.e. 1–5) tends to be un-modified or just slightly increased.

10969845, 0, Downloaded from https://onlinelibrary.wiley.com/doi/10.1002/eqe.4015 by CochraneItalia, Wiley Online Library on [23/09/2023]. See the Terms and Conditions (https://onlinelibrary.wiley.com/terms-and-conditions) on Wiley Online Library for rules of use; OA articles are governed by the applicable Creative Commons License

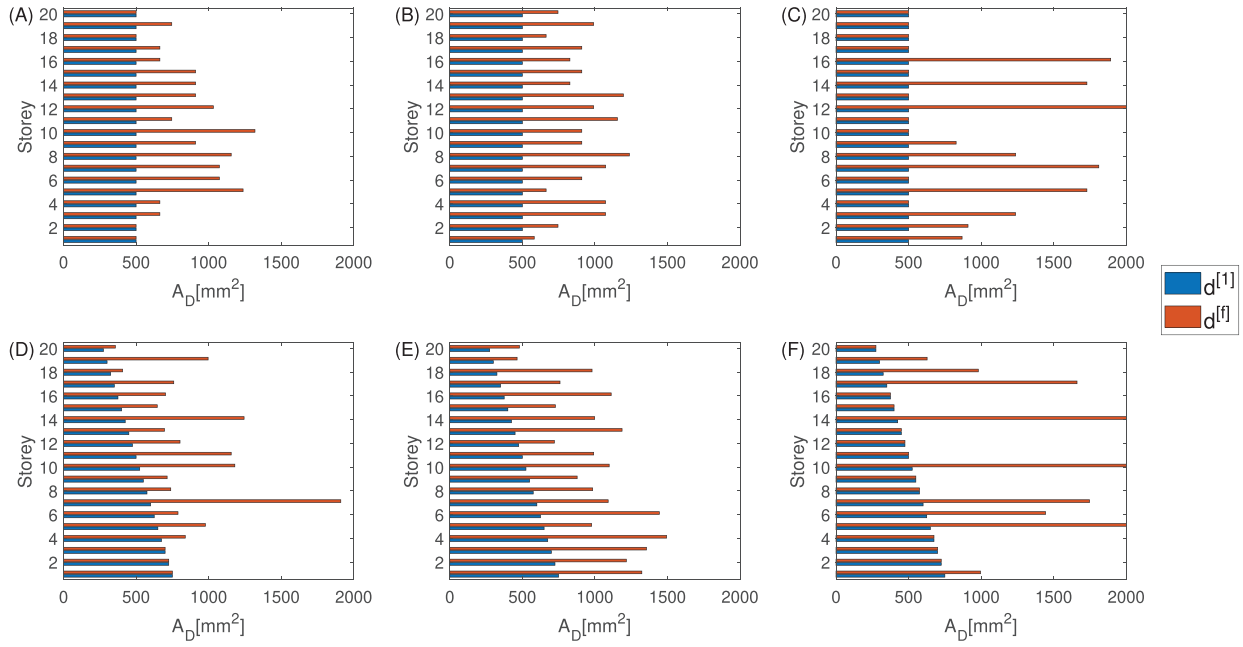


**FIGURE 6** Initial brace configuration $\mathbf{d}^{[1]}$ and final brace configuration $\mathbf{d}^{[f]}$: (A) Case $G_{1c}$; (B) Case $G_{2c}$; (C) Case $G_{3c}$; (D) Case $G_{1t}$; (E) Case $G_{2t}$; (F) Case $G_{3t}$.

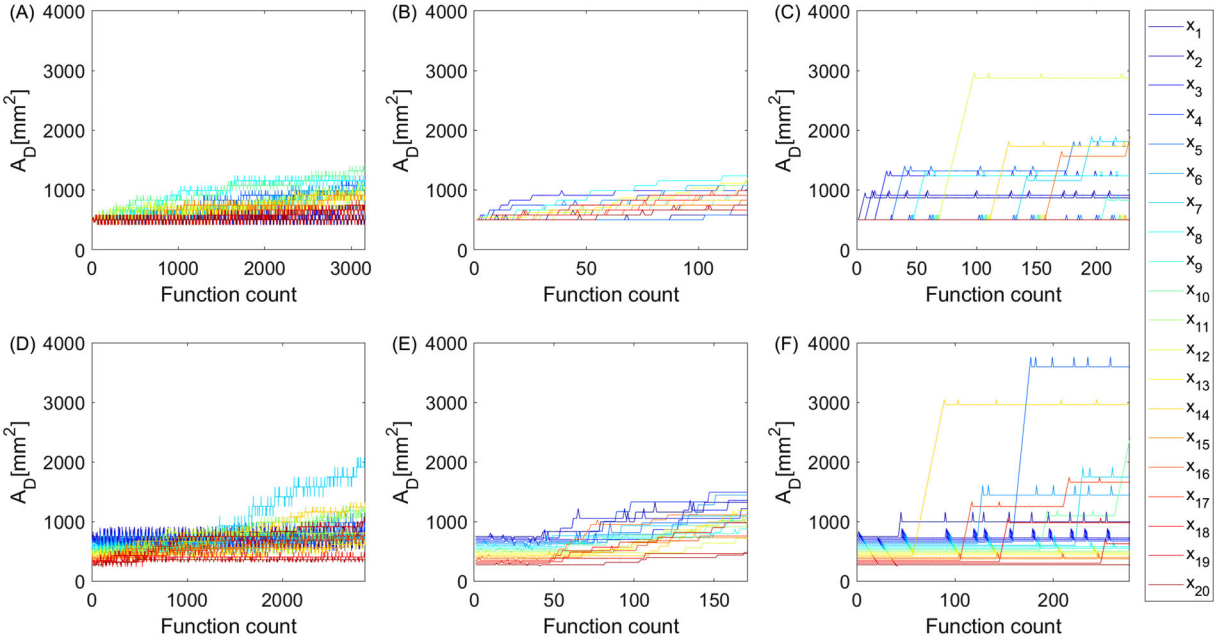


**FIGURE 7** Independent variables values versus number of FCs: (A) Case $G_{1c}$; (B) Case $G_{2c}$; (C) Case $G_{3c}$; (D) Case $G_{1t}$; (E) Case $G_{2t}$; (F) Case $G_{3t}$. FCs, Function Counts.

By looking at Figures 6B,E that show the $G_{2c}$ and $G_{2t}$ cases, it can be observed that there is a slight increase of all the variables, included lowest floors. In Figures 6C,F are shown the results obtained via "Success" strategy, in these cases the brace increase is provided only at specific floors where the brace areas reach values higher than 2000 mm$^2$ and are on purpose out of scale on the graph. On this point, Figure 7 shows the trends of the variables values during the optimization, it can be noticed how using Random OS (Figures 7B,E) a final solution very similar to "Full-Poll" (Figures 7A,B) can be obtained in much fewer iterations, while using "Success" strategy (Figures 7C,F) the final solution is very different from "Full-Poll" with just a few variables with very high values and other that are not modified during the process. The final

10969845, 0, Downloaded from https://onlinelibrary.wiley.com/doi/10.1002/eqe.4015 by CochraneItalia, Wiley Online Library on [23/09/2023]. See the Terms and Conditions (https://onlinelibrary.wiley.com/terms-and-conditions) on Wiley Online Library for rules of use; OA articles are governed by the applicable Creative Commons License

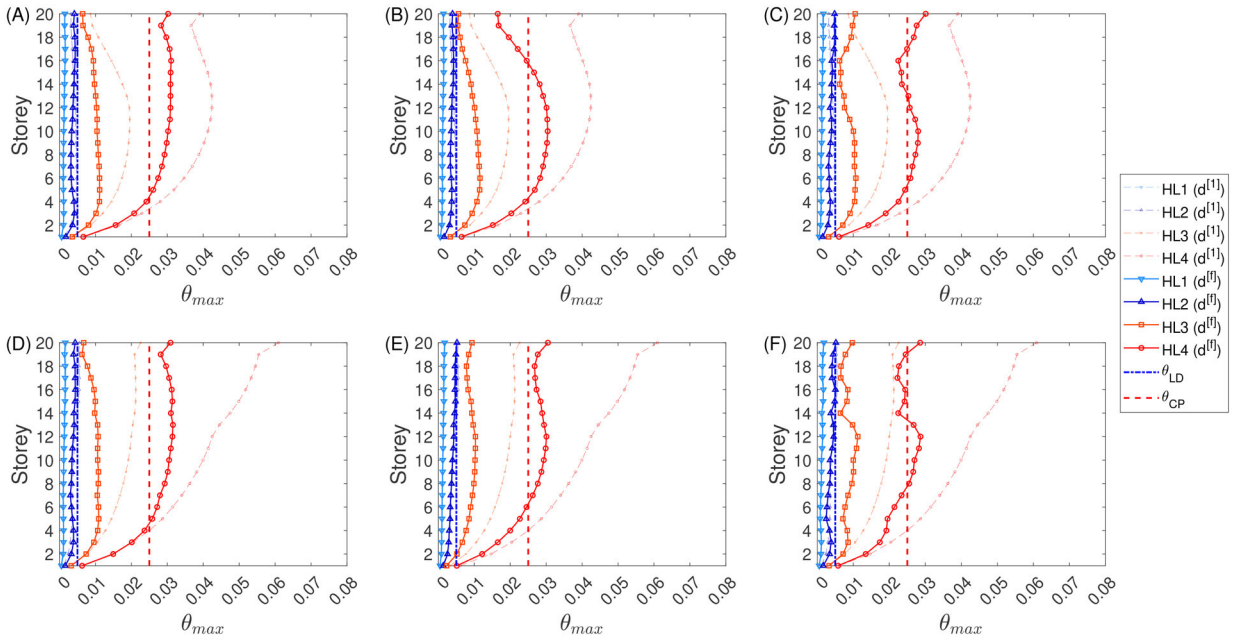


**FIGURE 8** $\theta_{max}$ for initial brace configuration $\mathbf{d}^{[1]}$ and final brace configuration $\mathbf{d}^{[f]}$: (A) Case $G_{1c}$; (B) Case $G_{2c}$; (C) Case $G_{3c}$; (D) Case $G_{1t}$; (E) Case $G_{2t}$; (F) Case $G_{3t}$.

solution provides different values of the dissipative area at each floor because variables are continuous. While this is not considered in this paper, the common design practice is to adopt a limited number of brace typologies along the height of the building. Practical design constraints like these can be implemented as a mapping from the vector of design variables to a reduced vector of basic design variables, as shown since the first version of the design procedure.[35] Table 3 also reports the sums of the brace volumes, V, assessed as the product of the brace areas and their length (i.e., $V = \sum_m A_{D,m} \times L_m$) for all the cases and it can be noticed that the by using the OS the final volume is higher than by using a Full-Poll. However, the volume increment with Random strategy is of 10% and 18% for $G_{2c}$ and $G_{2t}$, respectively, while using the "Success" strategy is 22% and 27% for $G_{3c}$ and $G_{3t}$, respectively.

Figure 8 shows the $\theta_{max}$ obtained through RSAs within the procedure, values obtained at the first iteration (i.e., $\mathbf{d}^{[1]}$) are shown in dashed lines and the values obtained at the last iteration (i.e., $\mathbf{d}^{[f]}$) are shown in solid lines. Looking at Figures 8A,D where the "Full-Poll" strategy cases are shown, it can be noticed that the final $\theta_{max}$ are pretty uniform along the height for all the HLs and are very similar among $G_{1c}$ and $G_{1t}$ cases, even if at the first iteration there are very different $\theta_{max}$ values. Figures 8B,E shows the solution for the "Random" strategy, in this case it can be noticed that $\theta_{max}$ have a reduction at highest floor but the final values by using two different initial points are pretty similar, also for these cases. Figure 8C,F shows the $\theta_{max}$ obtained for the "Success" strategy, in this case the $\theta_{max}$ are quite irregular along the height. In Table 3 are shown the final values of $\theta_{max}$ for all the HLs and it can be seen that even if the $\theta_{max}$ profiles differs among the various solutions, the maximum values are very similar. Figure 9 shows the equivalent damping values due to hysteresis (i.e., $\xi_h$) assessed within the procedure, it can be observed that the damping is null for an HL with $T_r = 100$ yrs and it gradually increases up to maximum values around 13% for $T_r = 10,000$ yrs. It can be further noticed that the equivalent damping assessment is quite similar between the different solutions.

The results described above allow to provide the following considerations:

- By using OSs there is a significant reduction of computational times, the total number of FCs required for the solution is always at least 90% less than in the case of "Full-Poll".
- The initial point adopted negligibly affects the speed of the procedure.
- The final elevation brace arrangement is very similar among the solutions, except for the case of "Success" strategy (i.e. $G_{3c}$ and $G_{3t}$). The total volume of the braces in "Full-Poll" cases are slightly lower than in the cases adopting OSs.
- The IDR profile appears as very uniform if the "Full-Poll" case is implemented, while it is highly irregular in the case of "Success" strategies.

10969845, 0, Downloaded from https://onlinelibrary.wiley.com/doi/10.1002/eqe.4015 by CochraneItalia, Wiley Online Library on [23/09/2023]. See the Terms and Conditions (https://onlinelibrary.wiley.com/terms-and-conditions) on Wiley Online Library for rules of use; OA articles are governed by the applicable Creative Commons License

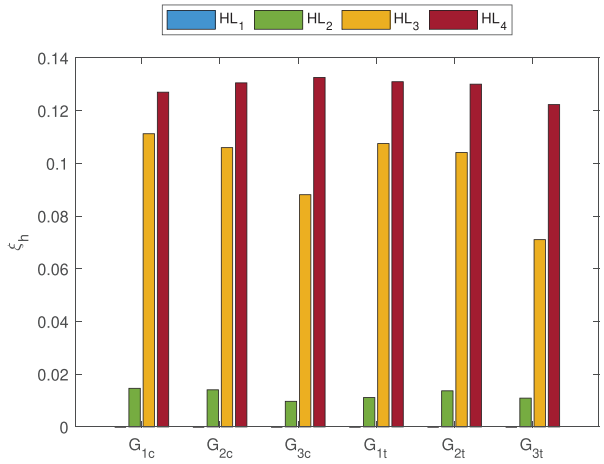


**FIGURE 9** Equivalent damping ratio due to hysteresis for the considered HLs. HLs, Hazard Levels.

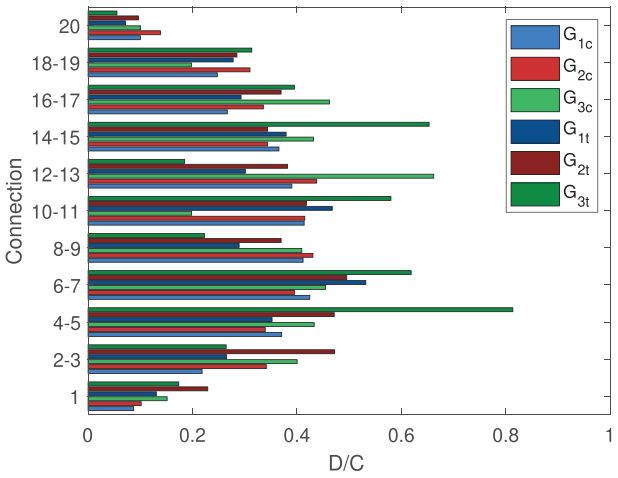


**FIGURE 10** Demand/Capacity ratio for the connections on the external columns.

In conclusion, it appears clear that the "Full-Poll" (i.e., $G_{1c}$ and $G_{1t}$) strategy provides the lowest values of volume and also a very uniform response along the height. Nevertheless, the "Random" OS (i.e., $G_{2c}$ and $G_{2t}$) appears promising because in front of a slight volume increment (i.e., $10\% - 18\%$) there is a very strong computational time reduction (higher than 90%). On the other hand, the "Success" strategy provides a significant volume increment (i.e., $22\% - 27\%$) and also a very irregular distribution of brace areas and IDR profiles, these two drawbacks make this solution unsuitable even if there is a big computational time reduction. According to these observations, the validation is conducted considering only the "Full-Poll" and "Random" in order to assess whether also NL analyses confirm the similarities of the structural responses obtainable with these two approaches.

As far as the connection feasibility is concerned, Figure 10 shows the demand to capacity ratio on the brace to column connection for each of the considered cases considering the capacity of the typological connection described in Section 2.2. Accordingly, Figure 10 shows the results for 11 connections, one every two floors plus one connection at the base and one at the roof. Capacity is higher than demand in all the cases, with ratios always lower than 0.6 for the "Full-Poll" and "Random" cases (i.e., $G_{1c}$, $G_{2c}$, $G_{1t}$, $G_{2t}$). Demand to capacity ratios obtained for the configurations designed through the "Success" strategy (i.e., $G_{3c}$, $G_{3t}$), on the other hand, are larger, up to 0.8, giving one more reason to rule out this strategy.

10969845, 0, Downloaded from https://onlinelibrary.wiley.com/doi/10.1002/eqe.4015 by CochraneItalia, Wiley Online Library on [23/09/2023]. See the Terms and Conditions (https://onlinelibrary.wiley.com/terms-and-conditions) on Wiley Online Library for rules of use; OA articles are governed by the applicable Creative Commons License

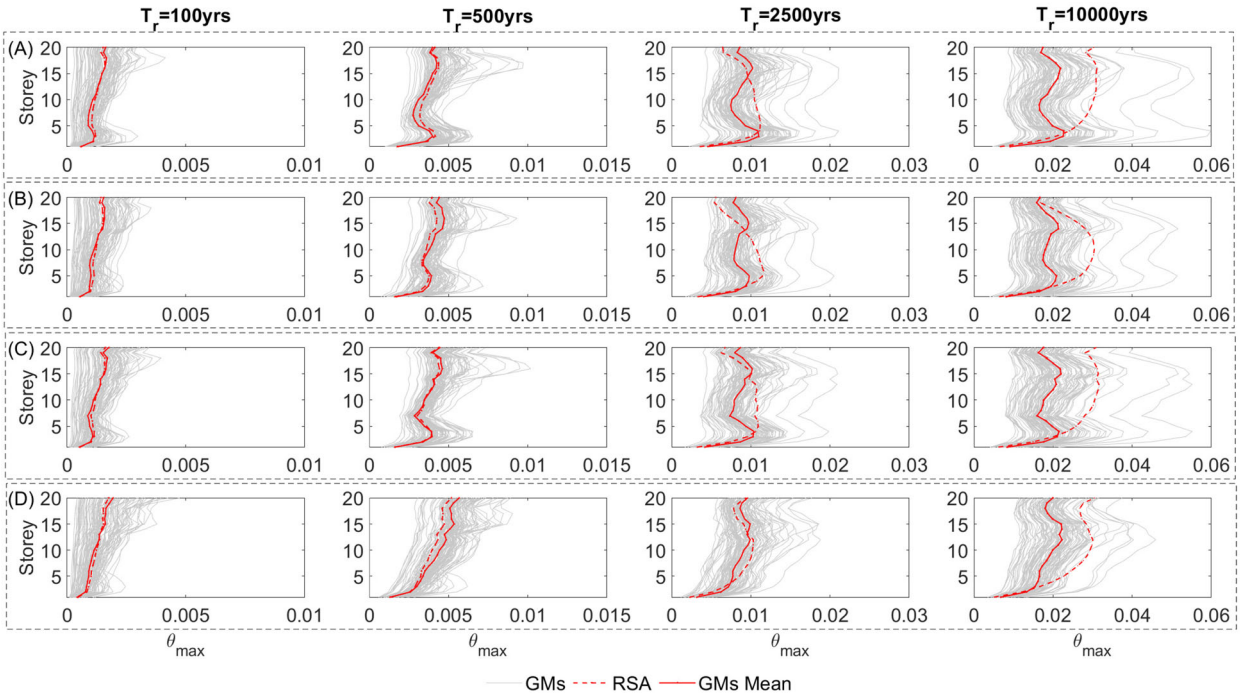


**FIGURE 11** $\theta_{max}$ derived from MSA and RSA: (A) Case $G_{1c}$; (B) Case $G_{2c}$; (C) Case $G_{1t}$; (D) Case $G_{2t}$. MSAs, Multiple Stripe Analyses; RSAs, Response Spectrum Analyses.

## 5 | NON-LINEAR TIME HISTORY ANALYSIS

This section shows the structural performance assessment obtained through MSAs and it also provides a comparison of such results with the ones obtained through RSAs and already discussed in Section 4.

The Non-Linear analyses are performed using Sap2000 software[75] and adopting the GMs set described in Section 2.3. BRB devices are modeled by using BRB element available within the library of Sap2000, the backbone curve of each brace is obtained using Equation (2) and the adopted hysteretic behavior considers only kinematic hardening. P-Delta effects have been considered, even if their influence should be significant only for the highest action level, given the relatively stiff structure. Damping has been modeled through a Rayleigh approach to obtain a value lower than 1% in a range of period between 0.5 s and 7 s. This value is slightly small for a TBs with such height, for whom the damping of the first mode can be estimated around 2%,[59] however given the high hysteretic damping contribution given by the braces, as illustrated in Figure 9, this underestimation of viscuous damping should not have excessively influenced the evaluation of the response, in particular for the higher intensity levels.

Figure 11 shows the values of $\theta_{max}$ obtained from MSAs for the considered design cases (i.e., $G_{1c}, G_{2c}, G_{1t}$ and $G_{2t}$) and for the four stripes corresponding to the HLs considered for RSAs (i.e., $T_r = 100$, $T_r = 500$, $T_r = 2500$ and $T_r = 10,000$ yrs). For the sake of comparison, Figure 11 shows also the $\theta_{max}$ obtained through RSAs for those HLs. The results show $\theta_{max}$ values quite uniform among all the considered design cases. By comparing RSAs (dashed red line) and MSAs mean values (solid red line) it can be seen that for HL with return periods up to $T_r = 500$ yrs the agreement is very good, for $T_r = 2500$ yrs the agreement is good in terms of maximum values but not in terms of IDR height profile. In particular, for $T_r = 2500$ yrs RSAs provide conservative results at the intermediate stories and slightly non-conservative results at higher stories. Finally, for $T_r = 10,000$ yrs MSAs show sensibly lower $\theta_{max}$ along almost all the height of the building, once again showing that RSAs with UHS provide conservative results relative to MSA with CMS with peak IDR overestimated of about 30% in all the cases. On this point it should be noticed that for such an high HL the fundamental period shifting is relevant, in fact the periods obtained on the linearized models for $T_r = 10,000$ yrs are higher than 6 s. In Figure 4B it can be noticed that the difference between PSHA and mean GMs spectra is comprised between 20% and 30% for a range of periods between 6 s and 7 s and thus partially justifies this difference in peak IDR assessment. Moreover, please note that GMs selection with multiple-CMS may have introduced some further bias, whilst a GMs selection with Conditional Spectrum (CS)[76–78] could have reduced these differences. The overall results show that RSAs provide a reliable assessment

10969845, 0, Downloaded from https://onlinelibrary.wiley.com/doi/10.1002/eqe.4015 by CochraneItalia, Wiley Online Library on [23/09/2023]. See the Terms and Conditions (https://onlinelibrary.wiley.com/terms-and-conditions) on Wiley Online Library for rules of use; OA articles are governed by the applicable Creative Commons License

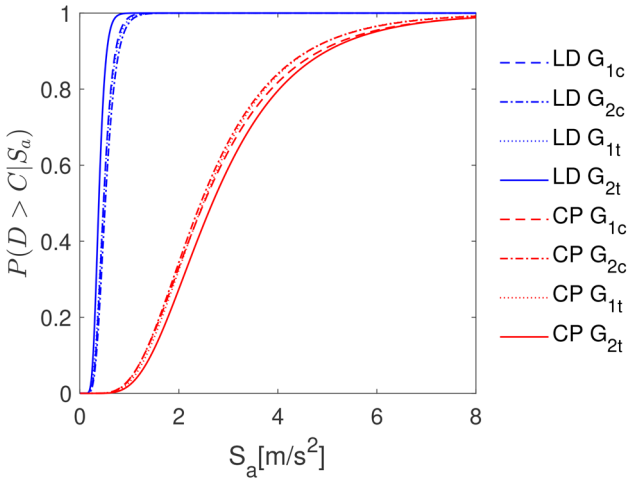


**FIGURE 12** Fragility curves for the four design cases.

**TABLE 4** Comparison of $\lambda$ values obtained through Response Spectrum and Multiple Stripe analyses and their threshold values.

| | $G_{1C}$ | $G_{2C}$ | $G_{1T}$ | $G_{2T}$ |
|---|---|---|---|---|
| $\lambda^*_{LD} \times 10^{-2}$ | 1.00 | 1.00 | 1.00 | 1.00 |
| $\lambda^{RSA}_{LD} \times 10^{-2}$ | 0.15 | 0.16 | 0.15 | 0.16 |
| $\lambda^{MSA}_{LD} \times 10^{-2}$ | 0.24 | 0.22 | 0.24 | 0.33 |
| $\lambda^*_{CP} \times 10^{-4}$ | 2.00 | 2.00 | 2.00 | 2.00 |
| $\lambda^{MSA}_{CP} \times 10^{-4}$ | 1.57 | 1.31 | 1.54 | 1.35 |
| $\lambda^{RSA}_{CP} \times 10^{-4}$ | 2.02 | 2.02 | 2.01 | 2.01 |

of peak IDR except for the case of $T_r = 10,000$ yrs, even if the height profiles show some differences in almost all the cases. Nevertheless, the height profiles provided by MSAs, even if less regular than the ones obtained through RSAs, proves to be quite uniform as demand increases, and does not show particular mechanisms or irregular responses even for very high HLs. Regarding the effectiveness of the different design cases, it can be noted that almost all of them provide very similar results and thus they appear to be equivalent, with the exception of $G_{2t}$ case that provide lower IDR at lowest stories but it anyhow provides very good agreement between MSAs and RSAs. On this point, observing Figure 6 it can be noticed that the $G_{2t}$ provides bigger braces at lower floors that, accordingly, provide stiffer response and, as far this case is concerned, provided a more regular response for the system.

Figure 12 shows the fragility curves obtained for the LD and CP LSs for the four considered design cases while in Table 4 are summarized the $\lambda_{LS}$ values obtained for the same design cases. The fragility curves tend to be very similar among the different cases and so are the $\lambda$ values, that is because the $\theta_{max}$ recorded on each design case are quite similar. By comparing the $\lambda$ values obtained through RSAs and MSAs exposed in Table 4, it can be noticed that the $\lambda_{LD}$ values obtained through MSAs are higher than the ones obtained through RSAs but still lower than design threshold (i.e., $\lambda^*_{LD} = 1 \times 10^{-2}$). On the other side, the $\lambda_{CP}$ values obtained through MSAs are lower than the ones obtained through RSAs, this is mainly related to the difference in $\theta_{max}$ assessment observed for $T_r = 10,000$ yrs that in turn provides lower values of frequency of exceedance. In any case, the $\lambda_{CP}$ values are lower the design threshold (i.e., $\lambda^*_{CP} = 2 \times 10^{-4}$), thus proving that the provided BRB systems allow to obtain the desired performance.

## 6 | CONCLUSIONS

This work presents a risk-based optimization procedure for the design of BRBs on tall TB. The procedure has been previously applied on RC buildings by using a gradient-based algorithm,[28] while in this paper it has been applied using a derivative free algorithm, the GPS. Such algorithm allows to solve non-linear non-convex problems guaranteeing convergence to a local minimum, however it can be highly time-consuming. In order to minimize the computational costs,

10969845, 0, Downloaded from https://onlinelibrary.wiley.com/doi/10.1002/eqe.4015 by CochraneItalia, Wiley Online Library on [23/09/2023]. See the Terms and Conditions (https://onlinelibrary.wiley.com/terms-and-conditions) on Wiley Online Library for rules of use; OA articles are governed by the applicable Creative Commons License

several solution approaches have been investigated by varying the initial points and using OS. Results show that using a "Random" opportunistic strategy computational costs can be reduced up to 96% with just a slight less refined solution, with an increase in the final volume of braces comprised between 12% and 18%. On the other side, the "Success" opportunistic strategy doesn't provide satisfying results, with an irregular distribution of braces resulting in a quite irregular structural response. Moreover, it should be observed that the initial point negligibly influences the solution, even if the cases with a constant initial distribution of variables provide lower final brace volume. All the solutions obtained satisfy the considered performance requirements for TBs and the force applied on the system by braces are compatible with doweled connection, thus not requiring specific design constraints, proving that this technology could be effective as a protection system for TBs even in the case of tall ones. MSAs show a good agreement with RSAs in terms of peak IDR assessment with the exception of the HL with $T_r$=10,000 yrs where differences are consistent but mainly related to different displacement demand obtained with uniform hazard spectra and selected GM records. Furthermore, the slight differences in terms of braces properties among the several approaches don't influence significantly the structural response, confirming that using a "Random" Opportunistic Strategy allows effective solution with small differences in terms of final structural response compared to "Full-Poll" approaches. In conclusion, this paper shows that BRBs are a viable solution to protect tall TBs, providing satisfying structural response and moderate force demand on the elements. Moreover, it has been shown how derivative free algorithm can be a very effective solution for the solution of the proposed optimization problem guaranteeing good convergence with reduced computational time if OS are adopted.

## ACKNOWLEDGMENTS

The financial support of the third author through Natural Science Engineering Research Council of Canada Discovery Grant (RGPIN-2019-05013) is acknowledged.

## CONFLICT OF INTEREST STATEMENT

The authors declare that they have no known competing financial interests or personal relationships that could have appeared to influence the work reported in this paper.

## DATA AVAILABILITY STATEMENT

The data that support the findings of this study are available from the corresponding author upon reasonable request.

## ORCID

*Raffaele Laguardia* https://orcid.org/0000-0003-3327-4844
*Paolo Franchin* https://orcid.org/0000-0002-1995-0415
*Solomon Tesfamariam* https://orcid.org/0000-0001-5353-5250

## REFERENCES

1. Svatoš-Ražnjević H, Orozco L, Menges A. Advanced timber construction industry: a review of 350 multi-storey timber projects from 2000–2021. *Buildings*. 2022;12(4):404.
2. Karacabeyli E, Gagnon S. *Cross Laminated Timber (CLT) Handbook*. FPInnovations; 2019.
3. Harte AM. Mass timber–the emergence of a modern construction material. *J Struct Integr Maint*. 2017;2(3):121-132.
4. Voulpiotis K, Schär S, Frangi A. Quantifying robustness in tall timber buildings: a case study. *Eng Struct*. 2022;265:114427.
5. Wilson AW, Phillips AR, Motter CJ, Lee JY, Dolan JD. Seismic loss analysis of buildings with post-tensioned cross-laminated timber walls. *Earthquake Spectra*. 2021;37(1):324-345.
6. Tesfamariam S. Performance-based design of tall timber buildings under earthquake and wind multi-hazard loads: past, present, and future. *Front Built Environ*. 2022;8:848698.
7. Canadian Commission on Building and Fire Codes (CCBFC), National Research Council of Canada (NRCC). *National Building Code of Canada (NBC)*. Ottawa, Canada. 2020.
8. Cover J. Mass timber: The new sustainable choice for tall buildings. *Int J High-Rise Build*. 2020;9(1):87-93.
9. Di Cesare A, Ponzo FC, Lamarucciola N, Nigro D. Experimental seismic response of a resilient 3-storey post-tensioned timber framed building with dissipative braces. *Bull Earthquake Eng*. 2020;18(15):6825-6848. https://doi.org/10.1007/s10518-020-00969-y
10. Ugalde D, Almazán JL, María HS, Guindos P. Seismic protection technologies for timber structures: a review. *Eur J Wood Wood Prod*. 2019;77:173-194. https://doi.org/10.1007/s00107-019-01389-9
11. Gallo PQ, Carradine DM, Bazaez R. State of the art and practice of seismic-resistant hybrid timber structures. *Eur J Wood Wood Prod*. 2021;79:5-28. https://doi.org/10.1007/s00107-020-01556-3
12. Gilbert CF, Erochko J. Development and testing of hybrid timber-steel braced frames. *Eng Struct*. 2019;198:109495.

10969845, 0, Downloaded from https://onlinelibrary.wiley.com/doi/10.1002/eqe.4015 by CochraneItalia, Wiley Online Library on [23/09/2023]. See the Terms and Conditions (https://onlinelibrary.wiley.com/terms-and-conditions) on Wiley Online Library for rules of use; OA articles are governed by the applicable Creative Commons License

13. Faggiano B, Iovane G, Salzillo D, Mazzolani FM, Landolfo R. Dissipative bracing systems for seismic upgrading of new and existing timber structures. *Int J Archit Herit*. 2021;15:289-312. https://doi.org/10.1080/15583058.2020.1830451
14. Hashemi A, Yousef-Beik SMM, Zarnani P, Quenneville P. Seismic strengthening of conventional timber structures using resilient braces. *Structures*. 2021;32:1619-1633. https://doi.org/10.1016/j.istruc.2021.03.100
15. Yousef-beik SMM, Bagheri H, Veismoradi S, Zarnani P, Hashemi A, Quenneville P. Seismic performance improvement of conventional timber brace using re-centring friction connection. *Structures*. 2020;26:958-968. https://doi.org/10.1016/j.istruc.2020.05.029
16. De Domenico D, Ricciardi G, Takewaki I. Design strategies of viscous dampers for seismic protection of building structures: a review. *Soil Dyn Earthquake Eng*. 2019;118:144-165. https://doi.org/10.1016/j.soildyn.2018.12.024
17. Whittle J, Williams M, Karavasilis T, Blakeborough A. A comparison of viscous damper placement methods for improving seismic building design. *J Earthquake Eng*. 2012;16(4):540-560. https://doi.org/10.1080/13632469.2011.653864
18. Zakian P, Kaveh A. Seismic design optimization of engineering structures: a comprehensive review. *Acta Mech*. 2023;234:1305-1330. https://doi.org/10.1007/s00707-022-03470-6
19. Filiatrault A, Cherry S. Seismic design spectra for friction damped structures. *J Struct Eng*. 1990;116:1334-1355. https://doi.org/10.1061/(ASCE)0733-9445(1990)116:5(1334)
20. Ciampi V, Angelis MD, Paolacci F. Design of yielding or friction-based dissipative bracings for seismic protection of buildings. *Eng Struct*. 1995;17:381-391. https://doi.org/10.1016/0141-0296(95)00021-X
21. Takewaki I. Optimal damper placement for minimum transfer functions. *Earthquake Eng Struct Dyn*. 1997;26(11):1113-1124. https://doi.org/10.1002/(SICI)1096-9845(199711)26:11<1113::AID-EQE696>3.0.CO;2-X
22. Garcia DL. A simple method for the design of optimal damper configurations in MDOF structures. *Earthquake spectra*. 2001;17(3):387-398. https://doi.org/10.1193/1.1586180
23. Levy R, Marianchik E, Rutenberg A, Segal F. Seismic design methodology for friction damped braced frames. *Earthquake Eng Struct Dyn*. 2000;29:1569-1585. https://doi.org/10.1002/1096-9845(200011)29:11<1569::AID-EQE960>3.0.CO;2-4
24. Moreschi LM, Singh MP. Design of yielding metallic and friction dampers for optimal seismic performance. *Earthquake Eng Struct Dyn*. 2003;32:1291-1311. https://doi.org/10.1002/eqe.275
25. Lavan O, Dargush GF. Multi-objective evolutionary seismic design with passive energy dissipation systems. *J Earthquake Eng*. 2009;13:758-790. https://doi.org/10.1080/13632460802598545
26. Pollini N, Lavan O, Amir O. Minimum-cost optimization of nonlinear fluid viscous dampers and their supporting members for seismic retrofitting. *Earthquake Eng Struct Dyn*. 2017;46:1941-1961. https://doi.org/10.1002/eqe.2888
27. Braga F, Gigliotti R, Laguardia R. Intervention cost optimization of bracing systems with multiperformance criteria. *Eng Struct*. 2019;182:185-197. https://doi.org/10.1016/j.engstruct.2018.12.034
28. Laguardia R, Franchin P. Risk-based optimization of bracing systems for seismic retrofitting of RC buildings. *J Struct Eng*. 2022;148(6):04022049. https://doi.org/10.1061/%28ASCE%29ST.1943-541X.0003335
29. Tu X, He Z, Huang G. Seismic multi-objective optimization of vertically irregular steel frames with setbacks upgraded by buckling-restrained braces. *Structures*. 2022;39:470-481. https://doi.org/10.1016/j.istruc.2022.03.044
30. Mazdarani MJH, Vaez SRH, Hosseini P, Fathali MA. Reliability-based layout optimization of concentrically braced in 3D steel frames. *Structures*. 2023;47:1094-1112. https://doi.org/10.1016/j.istruc.2022.11.130
31. Mam K, Douthe C, Le Roy R, Consigny F. Shape optimization of braced frames for tall timber buildings: Influence of semi-rigid connections on design and optimization process. *Eng Struct*. 2020;216:110692. https://doi.org/10.1016/j.engstruct.2020.110692
32. Pu W, Liu C, Dai F. Optimum hysteretic damper design for multi-story timber structures represented by an improved pinching model. *Bull Earthquake Eng*. 2018;16:6221-6241. https://doi.org/10.1007/s10518-018-0437-2
33. Cornell CA, Jalayer F, Hamburger RO, Foutch DA. Probabilistic basis for 2000 SAC Federal Emergency Management Agency steel moment frame guidelines. *J Struct Eng*. 2002;128(4):526-533. https://doi.org/10.1061/(ASCE)0733-9445(2002)128:4(526)
34. Jalayer F, Cornell C. Alternative non-linear demand estimation methods for probability-based seismic assessments. *Earthquake Eng Struct Dyn*. 2009;38(8):951-972.
35. Franchin P, Pinto PE. Method for probabilistic displacement-based design of RC structures. *J Struct Eng*. 2012;138:585-591. https://doi.org/10.1061/(asce)st.1943-541x.0000492
36. Franchin P, Petrini F, Mollaioli F. Improved risk-targeted performance-based seismic design of reinforced concrete frame structures. *Earthquake Eng Struct Dyn*. 2018;47(1):49-67. https://doi.org/10.1002/eqe.2936
37. Shibata A, Sozen MA. Substitute-structure method for seismic design in R/C. *J Struct Div*. 1976;102(1):1-18. https://doi.org/10.1061/JSDEAG.0004250
38. Vamvatsikos D. Derivation of new SAC/FEMA performance evaluation solutions with second-order hazard approximation. *Earthquake Eng Struct Dyn*. 2013;42(8):1171-1188. https://doi.org/10.1002/eqe.2265
39. Timmers M, Jacobs AT. Concrete apartment tower in Los Angeles reimagined in mass timber. *Eng Struct*. 2018;167:716-724. https://doi.org/10.1016/j.engstruct.2017.11.047
40. Zhou Y, Shao H, Cao Y, Lui EM. Application of buckling-restrained braces to earthquake-resistant design of buildings: a review. *Eng Struct*. 2021;246:112991. https://doi.org/10.1016/j.engstruct.2021.112991
41. Takeuchi T. Buckling-restrained brace: history, design and applications. *Key Eng Mater*. 2018;763:50-60. https://doi.org/10.4028/www.scientific.net/KEM.763.50


10969845, 0, Downloaded from https://onlinelibrary.wiley.com/doi/10.1002/eqe.4015 by CochraneItalia, Wiley Online Library on [23/09/2023]. See the Terms and Conditions (https://onlinelibrary.wiley.com/terms-and-conditions) on Wiley Online Library for rules of use; OA articles are governed by the applicable Creative Commons License

42. Wakabayashi M, Nakamura T, Katagihara A, Yogoyama H, Morisono T. Experimental study on the elastoplastic behavior of braces enclosed by precast concrete panels under horizontal cyclic loading-Parts 1 & 2. In: *Summaries of Technical Papers of Annual Meeting*. Vol. 6. Architectural Institute of Japan; 1973:121-128.
43. Della Corte G, D'Aniello M, Landolfo R, Mazzolani FM. Review of steel buckling-restrained braces. *Steel Constr*. 2011;4(2):85-93. https://doi.org/10.1002/stco.201110012
44. Uang CM, Nakashima M, Tsai KC. Research and application of buckling-restrained braced frames. *Int J Steel Struct*. 2004;4(4):301-313.
45. Zona A, Dall'Asta A. Elastoplastic model for steel buckling-restrained braces. *J Constr Steel Res*. 2012;68(1):118-125. https://doi.org/10.1016/j.jcsr.2011.07.017
46. Rahnavard R, Naghavi M, Aboudi M, Suleiman M. Investigating modeling approaches of buckling-restrained braces under cyclic loads. *Case Stud Constr Mater*. 2018;8:476-488. https://doi.org/10.1016/j.cscm.2018.04.002
47. Tremblay R, Poncet L, Bolduc P, Neville R, DeVall R. Testing and design of buckling restrained braces for Canadian application. In: *Proceedings of the 13th World Conference on Earthquake Engineering*. BC, Canada: Vancouver; 2004:1-16.
48. Tabatabaei SAR, Mirghaderi SR, Hosseini A. Experimental and numerical developing of reduced length buckling-restrained braces. *Eng Struct*. 2014;77:143-160. https://doi.org/10.1016/j.engstruct.2014.07.034
49. Hoveidae N, Tremblay R, Rafezy B, Davaran A. Numerical investigation of seismic behavior of short-core all-steel buckling restrained braces. *J Constr Steel Res*. 2015;114:89-99. https://doi.org/10.1016/j.jcsr.2015.06.005
50. Shemshadian ME, Razavi SA, Hosseini A, Mirghaderi SR, Mohammadi MK. An analytical study of low cycle fatigue effects in buckling restrained braces. In: *Proceedings of 3rd International Conference on Computational Methods in Structural Dynamics and Earthquake Engineering, COMPDYN*. Greece: Corfu; 2011.
51. Castellano MG. Italian experience in seismic retrofit of buildings through seismic isolation or energy dissipation. In: *Proceedings of the Third Conference on Smart Monitoring, Assessment and Rehabilitation of Civil Structures, SMAR*. Turkey: Antalya; 2015.
52. Antonucci R, Balducci F, Bartera F, Castellano MG, Fuller K, Giacchetti R. Shaking table testing of an RC frame with dissipative bracings. In: *Proceedings of the 13th world conference on Earthquake Engineering*. BC, Canada: Vancouver; 2004.
53. Vilguts A, Stamatopoulos H, Malo KA. Parametric analyses and feasibility study of moment-resisting timber frames under service load. *Eng Struct*. 2021;228:111583. https://doi.org/10.1016/j.engstruct.2020.111583
54. Shu Z, Li Z, He M, Zheng X, Wu T. Seismic design and performance evaluation of self-centering timber moment resisting frames. *Soil Dyn Earthquake Eng*. 2019;119:346-357. https://doi.org/10.1016/j.soildyn.2018.08.038
55. Dong W, Li M, Lee CL, MacRae G, Abu A. Experimental testing of full-scale glulam frames with buckling restrained braces. *Eng Struct*. 2020;222:111081. https://doi.org/10.1016/j.engstruct.2020.111081
56. CEN. *EN 1995-1-1: Eurocode 5: Design of timber structures - Part 1-1: General - Common rules and rules for buildings*. European Committee for Standardization. Brussels, BE. 2004.
57. Jacobsen LS. Steady forced vibration as influenced by damping. *TTrans Am Soc Mech Eng*. 1930;15:169-181. https://doi.org/10.1115/1.4057368
58. Jacobsen LS. Damping in composite structures. In: *Proceedings of the 2nd World Conference on Earthquake Engineering*. Tokyo and Kyoto, Japan; 1960:1029-1044.
59. Cruz C, Miranda E. Damping ratios of the first mode for the seismic analysis of buildings. *J Struct Eng*. 2021;147(1):04020300. https://doi.org/10.1061/(ASCE)ST.1943-541X.0002873
60. Smith R, Merello R, Willford M. Intrinsic and supplementary damping in tall buildings. *Proc Inst Civ Eng Struct Build*. 2010;163(SB2):111-118.
61. Aloisio A, Alaggio R, Fragiacomo M. Equivalent viscous damping of cross-laminated timber structural archetypes. *J Struct Eng*. 2021;147(4):04021012. https://doi.org/10.1061/(ASCE)ST.1943-541X.00029
62. Bommer JJ, Elnashai A, Weir AG. Compatible acceleration and displacement spectra for seismic design codes. In: *Proceedings of the 12th World Conference on Earthquake Engineering*. New Zealand: Auckland; 2000:1-8.
63. GEM (Global Earthquake Model). OpenQuake Manual for Engine version 3.17.2. 2023. Accessed July 25, 2023. https://docs.openquake.org/manuals/OpenQuake
64. Kolaj M, Allen T, Mayfield R, Adams J, Halchuk S. Ground-motion models for the 6th Generation Seismic Hazard Model of Canada. In: *Proceedings of the 12th Canadian Conference on Earthquake Engineering*. Quebec, Canada: Chateau Frontenac; 2019.
65. Baker JW. Conditional mean spectrum: tool for ground-motion selection. *J Struct Eng*. 2011;137:322-331. https://doi.org/10.1061/(ASCE)ST.1943-541X.0000215
66. Goda K, Atkinson GM. Seismic performance of wood-frame houses in south-western British Columbia. *Earthquake Eng Struct Dyn*. 2011;40(8):903-924. https://doi.org/10.1002/eqe.1068
67. DeVall RH. Background information for some of the proposed earthquake design provisions for the 2005 edition of the National Building Code of Canada. *Can J Civ Eng*. 2003;30:279-286. https://doi.org/10.1139/l02-048
68. Federal Emergency Management Agency (FEMA). *FEMA P695. Quantification of Building Seismic Performance Factors*. Applied Technology Council (ATC). Redwood City CA, USA; 2009.
69. NIST. Evaluation of the FEMA P-695 methodology for quantification of building seismic performance factors. Report n. GCR 10-917-8. *Prepared for the US National Institute of Standards and Technology by the NEHRP Consultants Joint Venture, Gaithersburg*. Gaithersburg, MD; 2010. Accessed May 16, 2023. https://tsapps.nist.gov/publication/get_pdf.cfm?pub_id=915492
70. Hare W, Nutini J, Tesfamariam S. A survey of non-gradient optimization methods in structural engineering. *Adv Eng Software*. 2013;59:19-28. https://doi.org/10.1016/j.advengsoft.2013.03.001
71. Hooke R, Jeeves TA. "Direct search" solution of numerical and statistical problems. *J ACM (JACM)*. 1961;8(2):212-229.


10969845, 0, Downloaded from https://onlinelibrary.wiley.com/doi/10.1002/eqe.4015 by CochraneItalia, Wiley Online Library on [23/09/2023]. See the Terms and Conditions (https://onlinelibrary.wiley.com/terms-and-conditions) on Wiley Online Library for rules of use; OA articles are governed by the applicable Creative Commons License

72. Torczon V. On the convergence of pattern search algorithms. *SIAM J Optim*. 1997;7(1):1-25. https://doi.org/10.1137/S1052623493250780
73. Hare W, Audet C. *Derivative-Free and Blackbox Optimization*. Springer; 2017. https://doi.org/10.1007/978-3-319-68913-5
74. McKay MD, Beckman RJ, Conover WJ. A comparison of three methods for selecting values of input variables in the analysis of output from a computer code. *Technometrics*. 1979;21(2):239-245. https://doi.org/10.1080/00401706.2000.10485979
75. Computers and Structures Inc. (CSI). SAP2000 v20.2.0. Berkeley CA, USA. 2018 European Committee for Standardization.
76. Lin T, Haselton CB, Baker JW. Conditional spectrum-based ground motion selection. Part I: hazard consistency for risk-based assessments. *Earthquake Eng Struct Dyn*. 2013;42(12):1847-1865. https://doi.org/10.1002/eqe.2301
77. Lin T, Haselton CB, Baker JW. Conditional spectrum-based ground motion selection. Part II: intensity-based assessments and evaluation of alternative target spectra. *Earthquake Eng Struct Dyn*. 2013;42(12):1867-1884. https://doi.org/10.1002/eqe.2303
78. Lin T, Harmsen SC, Baker JW, Luco N. Conditional spectrum computation incorporating multiple causal earthquakes and ground-motion prediction models. *Bull Seismol Soc Am*. 2013;103(2A):1103-1116. https://doi.org/10.1785/0120110293


**How to cite this article:** Laguardia R, Franchin P, Tesfamariam S. Risk-based optimization of concentrically braced tall timber buildings: Derivative free optimization algorithm. *Earthquake Engng Struct Dyn*. 2023;1-21. https://doi.org/10.1002/eqe.4015

10969845, 0, Downloaded from https://onlinelibrary.wiley.com/doi/10.1002/eqe.4015 by CochraneItalia, Wiley Online Library on [23/09/2023]. See the Terms and Conditions (https://onlinelibrary.wiley.com/terms-and-conditions) on Wiley Online Library for rules of use; OA articles are governed by the applicable Creative Commons License